# Investigating the secondary electron emission of nanomaterials induced by a high resolution proton beam

M. Cholewa[*1], A. Grędysa[1], A. Pozaruk[1], T. Osipowicz[2], J. A. van Kan[2], Y. X. Dou[2], P. Y. Yan[2], A. A. Bettiol[2], I. Maximov[3], M. Sobanska[4], Z. R. Zytkiewicz[4], N. Gogneau[5], M. Tchernycheva[5], K. Lee[6], M. S. Song[6], G.-C. Yi[6], P. Boutachkov[7]

[1]Institute of Physics, College of Natural Sciences, University of Rzeszów, Pigonia Street 1, 35-959 Rzeszów, Poland
[2]Centre for Ion Beam Applications, Department of Physics, National University of Singapore, 2 Science Drive 3, Singapore 117542
[3]Lund Nano Lab, Division of Solid State Physics and NanoLund, Lund University, Box 118, S-22100, Lund, Sweden
[4]Institute of Physics, Polish Academy of Sciences, Al. Lotnikow 32/46, 02-668 Warsaw, Poland
[5]Centre for Nanoscience and Nanotechnology (C2N), Université Paris-Saclay, Route de Nozay, F-91460 Marcoussis, France
[6]Seoul National University, Dept. of Physics and Astronomy, Institute of Applied Physics and Research Institute of Advanced Materials, Seoul 151-747, Republic of Korea
[7]GSI Helmholtzzentrum für Schwerionenforschung GmbH, Planckstraße 1, 64291 Darmstadt, Germany

**Abstract**

In this article the Secondary Electron Emission (SEE) from 1-dimensional (1D) nanomaterials in the form of nanorods are investigated. The small beam of a 1.5 MeV + H2 hydrogen with a sub 70 nm in diameter allowed studying the SEE with a very high resolution. A wide range of nanomaterials from various laboratories were studied, including thin ZnO and ZnO/GaN nanostructures grown on 1 μm thick Si3N4 membranes and thick InP, GaN and GaN/AlN nanorod structures grown on bulk Si substrates. By virtue of the small size of the exciting nanobeams, high resolution maps could be created presenting an SEE yield from various parts of the structures. This allowed us to show that the top parts of nanorods in ZnO, ZnO/GaN, GaN, InP and GaN/AlN nanostructures emit secondary electrons much more efficiently than the valley areas between nanorods. These results indicate that by a proper design and growth of 1D nanostructures, SEE properties could be improved over those of the traditionally used Au and CsI thin films. This work has been undertaken to find materials with the highest achievable SEE emission, which is a figure of merit for the detection efficiency relevant for the development and application of novel radiation detectors.

[*]Corresponding author: Marian Cholewa (mcholewa@ur.edu.pl)

## Introduction

The primary motivation for this work has been the need for the development of highly efficient radiation detectors in various fields, from space application(s) to environmental research. The nanomaterials investigated possess geometric structural detail that is expected to improve their SEE properties over those of blank thin film/bulk materials. Here, we present results for several nanostructured materials, as derived from MeV ion nanoprobe irradiation(s) performed at the best lateral resolutions available [CIBA].

A vast amount of work has been performed for the development and characterization of the physical properties of CNTs (carbon nanotubes)[1-3] and NNs (nanoneedles)[4,6,7] as well as for their field emission capabilities. This research has mostly been driven by the need for the development of next generation flat screen displays. However, to the best of our knowledge, there has been very little research[8-10] on these nanomaterials regarding their SEE properties and their potential for novel advanced detectors of ionizing radiation.

Conversely, during recent decades some scientific research[11-17] has been focused on material properties for obtaining anti-multipactor coatings for low SEE. Both the High Energy Physics community and the European Space Agency (ESA) have been pushing research towards a new approach to this problem based on engineered surface roughness, that might act as a Faraday cage and reduce electron emission. Several groups[11,12] have been working on the development of efficient techniques to reduce the SEE (also known as Secondary Electron Yield - SEY or $\delta$) from beam line components made of stainless steel, copper or aluminum. In several studies[11,12] authors have shown considerable reduction of the SEE by the introduction of micro or nanostructures to the surfaces of stainless steel, copper or aluminum through a nanosecond pulsed laser irradiation process. The effects of such complex surfaces on the vacuum properties of complex vacuum systems have been investigated through a simplified 2D theoretical model[13] of the molecular pumping properties.

In a different project, a multilayer coating structure[14] was adopted to comply with the stringent requirements for space applications. The surface of a standard silver plating was modified via a two-step treatment, wet etching and Au magnetron sputtering. The resulting nanostructure was efficient in reducing the SEE properties of the surface. Another group[15] performed numerical simulations on complex structures called velvet structures (vertically standing whiskers) and developed an approximate analytical model that calculates the net secondary SEE yield from a velvet surface as a function of the velvet whisker length and packing density, and the angle of incidence of primary electrons. The reduction in the SEE occurs due to the efficient capture of low-energy, true secondary electrons emitted at the bottom of the structure and on the sides of the velvet whiskers. Among all the known SEE suppression techniques, micro-porous surfaces are perhaps the most efficient. In a recent paper[16] the authors developed an analytical model that approximates contributions to the total SEE from both the 1st and 2nd generation secondary electrons produced, showing that complex structures at the surface can significantly reduce the total SEE. This reduction occurs due to the capture of low-energy, true secondary electrons emitted at one point of the structure and intersecting another. In a further study[17], Monte Carlo calculations were used to demonstrate that fractal structured surfaces can efficiently reduce the total SEE produced, as compared to the flat surface.

**Work to Decrease SEE**

In a number of studies[1-17], several experimental and theoretical approaches to investigate the SEE properties of micro/nanomaterials were taken. In these papers the authors try to develop structures that will reduce SEE properties.

Authors are trying to develop suppressing layers on different materials including stainless steel, copper and aluminum.

**Work to Increase SEE**

In our research[8-10] we are trying to develop and investigate nanostructures made of different nanomaterials, including ZnO, ZnO/GaN, GaN, InP and GaN/AlN, that will show an increase in the SEE properties.

Both of these research directions are valuable, and the results are complementary. It is expected that a full picture of the SEE properties will emerge from this work.

Cholewa and the Singapore Synchrotron Light Source (SSLS) group received a patent in the USA[9] ("Radiation Detector Having Coated Nanostructure and Method", United States Patent No. 7,388,201 (June 17, 2008)) for the development of a prototype radiation detector, based on selected nanomaterials. Further development will be necessary to develop radiation detectors for specific applications (e.g., with large radiation resistance). The work presented here is a study of very basic properties for SEE.

This article does not compare the performance of modified surfaces with their flat and unmodified counterparts. However, such work was reported in references[8] where performances of ZnO, ZnO/GaN and ZnO/AlN nanostructures were investigated, with the conclusion that nanostructures performed much better than flat samples. Therefore, we have decided not to repeat previous results, but perform a comparable study with a flat Au surface only.

Moreover, the aim of this paper is not to give a detailed description of how to develop radiation detectors based on selected nanomaterials, but to demonstrate this possibility and indicate its potential advantages.

Since 1995, M. Cholewa, with collaborators, have conducted preliminary research[8-10] on SEE properties of a number of nanomaterials such as boron-doped polycrystalline diamond[5-7] and 1D nanostructures of ZnO, ZnO/AlN and ZnO/GaN[8-10]. Both classes of materials have been extensively studied in laboratories worldwide (Philips, Samsung and other institutes/companies), due to possible commercial applications in flat screen displays. This work was continued from 2016 as part of the EU project ENSAR2 (http://www.ensarfp7.eu) in cooperation with groups from Poland, France, Germany, Korea, Singapore and Sweden. Despite progress made, an in-depth understanding on the emission of secondary electrons from nanostructures is still elusive. The remaining questions are important, in terms of both fundamental research and application development.

As a reference[8], experiments with many beams were compared: X-rays (SSLS Singapore); heavy ions (at GSI, Darmstadt, Germany); electrons (GSI, Darmstadt) and MeV alpha particles; focused microbeams at CIBA at the NUS.

This work does not fully explain the SEE properties of the selected nanomaterials, because it is not clear if the observed SEE enhancement is a function of the nanostructures only, or if other factors are relevant. We are planning more detailed theoretical and experimental works on this topic in the future.

## Experimental Methods

Details of the Centre for Ion Beam Applications (CIBA) nanoprobe focusing system at NUS can be found in the accompanying references/literature[18,19]. Though, essentially, the system contains a single ended 3.5 MeV SINGLETRON accelerator and three associated nanoprobe beam-lines. A beam of 1.5 MeV $^{+}H_2$ was used for SEE excitation. In order to obtain the small beam spot size, a magnetic quadrupole triplet focusing system was aligned with object apertures of 8μm x 3μm and collimator apertures of 20μm x 20 μm. This allowed us to utilize beam sizes below 70 nm in diameter during all experiments discussed in this study. This was not the best achievable resolution of the system, a consequence of the fact that the accelerator radiofrequency ion source was in a sub-optimal condition and delivered a beam brightness less than 10 A/m$^2$srV. However, the resolutions achieved were fully sufficient to achieve the aims of this study. Under ideal circumstances, with a beam brightness of 42 A/(m$^2$srV), the CIBA automatic focusing system allows the beam to be focused[20] to 23 x 32 nm$^2$.

Figure 1 shows the experimental setup and the beam incidence scheme used in this study. The secondary electrons emitted from the sample were detected by a micro-channel-plate (MCP) detector (model NVT2C45/C4M10 – NVT). The MCP had a Chevron configuration with detection channels a diameter of 10 μm, spaced 15 μm apart. When testing thin samples transparent for the beam, the transmitted ions were recorded by a PIN diode (model S1223-Hamamatsu). Then the recorded counts from the MCP detector were normalized to the number of counts from the PIN diode detector. For the SEE measurements of samples grown on bulk substrate non-transparent for the ion beam (hereafter named thick samples), only the number of secondary electron counts were recorded by the MCP. In these cases, we normalized the MCP signal to the exposure time assuming a constant beam current during the experiment. Unfortunately, this might possibly lead to some uncertainties of results. However, our studies of thin samples indicated quite a high stability of the incident beam within the time of our experimental session.

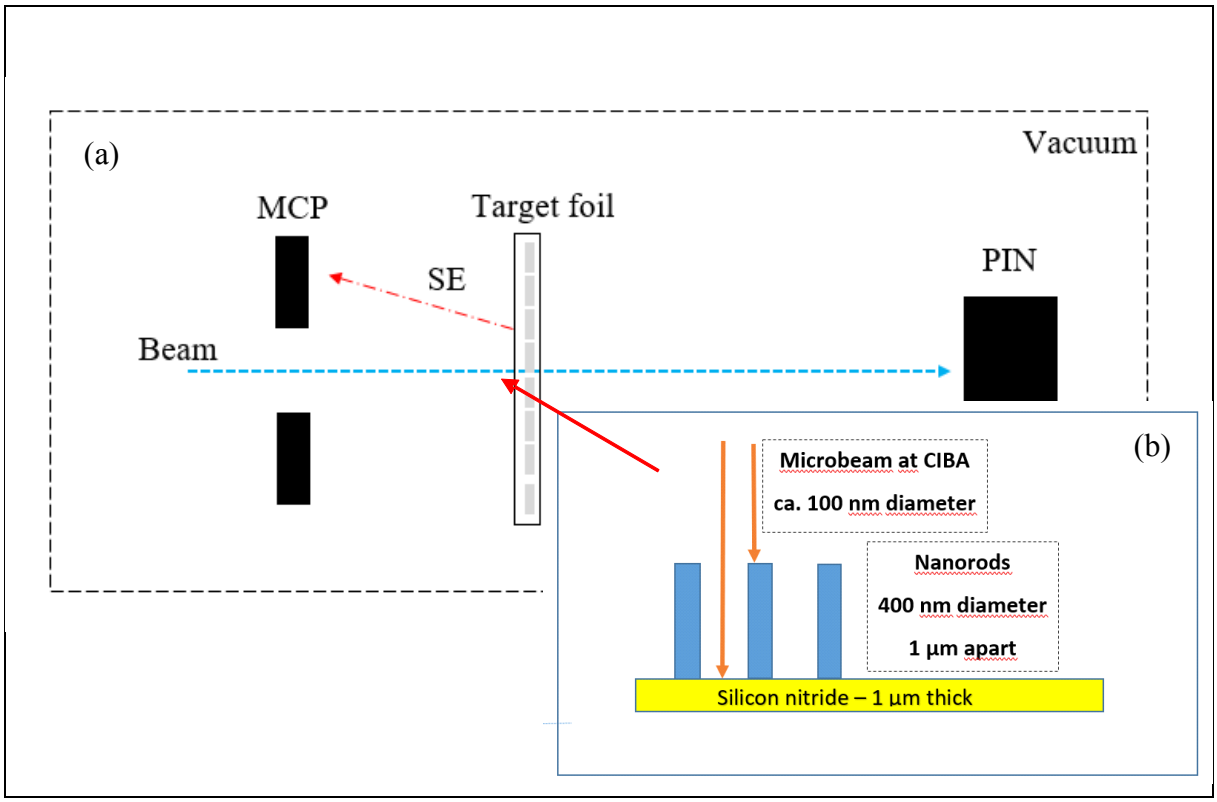


**Figure 1:** Set-up of the two detectors (PIN diode and MCP) in relation to the incoming beam of $^{+}H_2$ is shown in (a). PIN diode registered the incoming ions and MCP counted the number of generated secondary electrons. Insert (b) shows the structure of 5 µm long ZnO/GaN nanorods with a ~1 µm diameter and spaced at ~1 µm.

The MCP was placed about 8 mm from the sample surface while the PIN diode was located about 100 mm behind the sample. Object slits were open at 8µm x 3µm and collimator slits were open at 20µm x 20 µm - this led to the beam size being smaller than 70 nm in diameter. Figure 1(b) shows the position of the sample during the experiment. Both thin and thick samples were tested. As an example, the schematic drawing of 1D ZnO nanorods on 1 µm thick $Si_3N_4$ membrane is presented. The Au sample containing the 20 nm thick gold layer on a 1 µm thick $Si_3N_4$ membrane was used as the reference material and compared with all other samples.

It is worth mentioning that a similar geometry has been utilized at CIBA for high resolution (down to 20 nm structure sizes) proton beam writing[21]. The technique is based on the effect that fast protons reaching the target lose their energy mainly through proton-electron interactions. Due to the much higher mass of protons than electrons (about 1,800 times), protons transfer less than 100 eV energy to individual secondary electrons. The scattering of protons in the target is negligible, and hence nearly all protons reach the PIN diode detector. The beam current was below 10 fA to reduce the count rate and possible damage to the particle detector, which was positioned at 0 degrees behind the sample.

## Sample Preparation

Two types of samples were used in this study. Thin ZnO and ZnO/GaN samples were grown on a commercial 1 μm thick $Si_3N_4$ membrane (from Silson Ltd.) on which thin graphene film was transferred from the host Cu foil. Further, the substrate was covered by a 300 nm thick $SiO_2$ masking layer in which mask-free openings were formed by a conventional lithography technique and etching. Finally, ZnO arrays of 5 μm long nanorods of 400 nm in diameter and spaced at 1 μm were grown on such substrates by metal-organic vapor phase epitaxy (MOVPE) using a selective area growth mode. Heteroepitaxy of n-GaN on ZnO was performed by a two-step MOCVD growth method to form a 10 nm thick GaN shell coating ZnO nanorod cores. More details on the growth of ZnO and ZnO/GaN samples are presented in associated works[22-25].

In addition to thin samples, the selected arrays of nanorods of other materials grown on bulk substrates (thick samples) were also tested for their SEE efficiency. These included InP samples delivered by Lund University, which had regular arrays of undoped InP nanorods grown by MOVPE with the use of Au seed particles to nucleate the selective growth on the InP substrate. The 1.3 μm long nanorods had a diameter of 215 nm and were arranged in a hexagonal pattern[26] with a pitch of 0.5 μm. Due to the production process, the top of the InP nanorod was covered by a small gold amount.

A GaN/AlN self-assembled nanorod structure was delivered by the Institute of Physics of the Polish Academy of Sciences in Warsaw, Poland. First, 1 μm long GaN nanorods were formed on nitridated n-type Si (111) substrates by plasma-assisted molecular beam epitaxy (PAMBE) without using a catalyst. This was followed by the axial growth of a 100 nm long AlN part. No intentional doping was used. More details on the growth procedure used can be found elsewhere[27-31].

GaN nanorods grown by catalyst-free PAMBE on a Si (111) substrate in similar ways as above were delivered by the Centre for Nanoscience and Nanotechnology (C2N) in Paris, France[32].

After growth, all samples were studied by scanning electron microscopy (SEM) to gain insight into their surface morphology, and to measure characteristic dimensions of the nanostructures.

## Results

All samples were studied to determine the efficiency of secondary electron production. The analysis of the results was based on the data generated by the data acquisition software (OMDAQ) available at CIBA. This program generates list mode data, so the information on the number of particles counted by both the PIN diode and the MCP detector can be recorded as the beam scans the sample. For offline analysis, OCTIVE software was used to construct quantitative maps of spatial distribution of the SEE signal from the samples.

Figure 2(A) shows a SEM image of ZnO nanorods coated by a 10 nm thick GaN shell grown on a 1 μm thick $Si_3N_4$ membrane. As seen here, the nanorods are perpendicular to the substrate and are well organized into a square matrix. Moreover, a high growth selectivity has been achieved. Figure 2(B) shows the map of secondary electrons collected from the scan area of

11.0 x 11.0 μm$^2$. The beam spot size in this experiment was sub 70 nm in diameter, and the color bar on the right of the picture shows the intensity scale. As seen here, the map corresponds well to the surface morphology of the sample. Moreover, brighter color at the nanorods' positions indicates a much larger secondary electron yield from the top of the nanorods than from the valleys in between them.

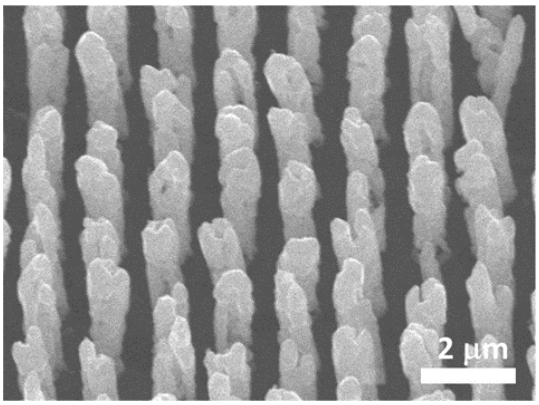


Figure 2A

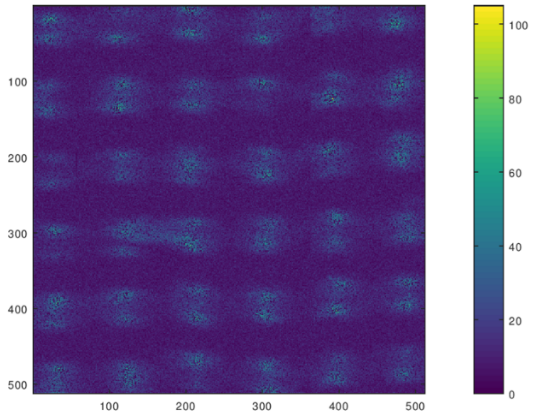


Figure 2B

**Figure 2 (2A):** SEM picture of nanorods of ZnO with 10 nm thick GaN coating are 1 μm apart, 1 μm in diameter and 5 μm in length. They are perpendicular to the surface and developed on the 1 μm thick $Si_3N_4$ membrane from SILSON Ltd. Figure 2B shows the number of secondary electrons detected by the MCP detector from of the scan of the 1.5 MeV $^+H_2$ beam on the ZnO/GaN thin sample. The scan was 11.0 x 11.0 μm$^2$. In this experiment the beam size was sub 70 nm in diameter. This picture shows no uniform signal from the top of the nanorods which corresponds effectively with the SEM picture of this sample presented in Figure 2A.

Figure 3A shows a SEM image of the InP nanorods grown by MOVPE on a bulk InP substrate. The nanorods have a diameter of 215 nm and are well organized, in a hexagonal array, with a 500 nm period. Au droplets used for selective area vapor-liquid-solid growth of nanorods are visible on their top facets. Figure 3B shows the secondary electron emission map from the sample. The beam spot size was sub 70 nm in diameter, and the color bar on the right shows the intensity scale. As before, a brighter color at the positions corresponding to nanorods indicate a much larger secondary electron yield from the top of the nanorods than from the valleys in between them.

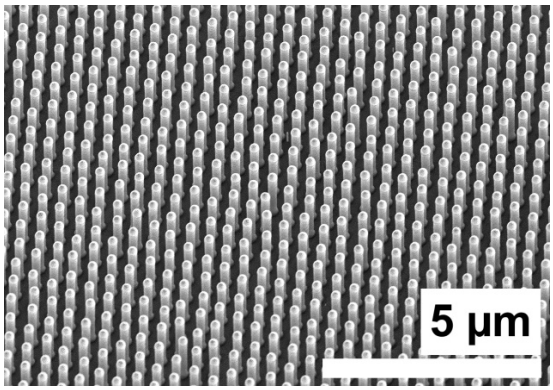


Figure 3A

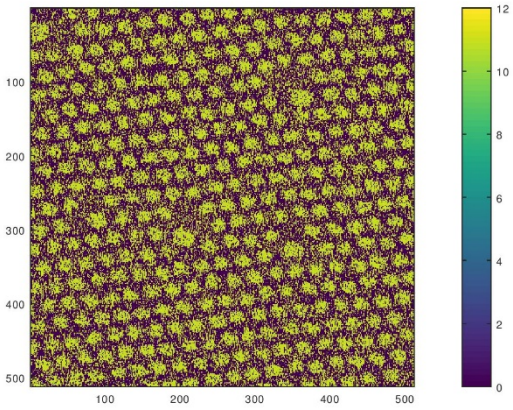


Figure 3B

**Figure 3 (3A):** SEM image of the sample with InP nanorods on bulk InP substrate; (3B): the map showing spatial distribution of the number of secondary electrons recorded by the MCP detector during scan of the proton beam on the InP thick sample. The beam size was sub 70 nm in diameter and the scan area was 11.0 x 11.0 $\mu m^2$. The color bar to the right of the map shows the intensity scale.

Finally, figure 4(A) shows a top view of the SEM image of GaN/AlN nanorod structure grown by PAMBE on a bulk Si (111) substrate. Since the nanorods are nucleated in self-assembly mode they are not as regularly distributed over the substrate surface as those presented in Fig. 2 and 3 formed by the/a selective area growth. Due to a large length (2.4 µm), small diameter (~70 nm) and high density, some coalescence of neighboring nanorods is clearly visible in the image. Therefore, top facets of the nanorods are not regular hexagons but have a shape of clusters with the average size of ~200 nm.

Figure 4(B) shows the secondary electron emission map of the sample. The beam spot size was sub 100 nm in diameter and the color bar on the right shows the intensity scale. As before, the map adequately reproduces the morphology of the sample indicating secondary electron emission, mainly from the top of the nanorods. This time however, the contrast in electron emission intensity map, i.e., the ratio of SEE signals from nanorod tops and valleys is significantly larger than in the previous two cases.

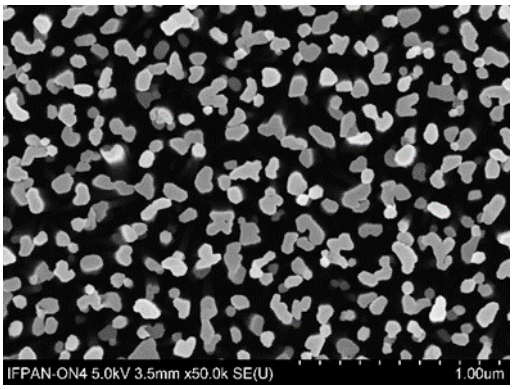


Figure 4A

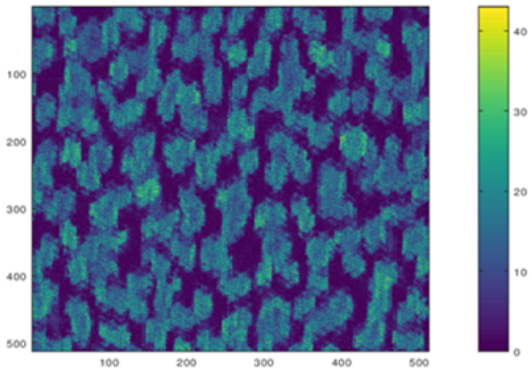


Figure 4B

**Figure 4 (4A):** top view SEM image of GaN/AlN nanorod structure on bulk Si (111) substrate; (B) the map showing spatial distribution of the number of secondary electrons recorded by the MCP detector during scan of the proton beam on the GaN/AlN thick sample. The beam size was sub 70 nm in diameter and the scan area was 11.0 x 11.0 $\mu m^2$. The color bar on the right of the map shows the intensity scale.

The reconstruction of the maps allowed us to accurately analyze the number of counted particles and electrons, both from the top of the nanowires themselves, and from the valleys between them. Due to the very high spatial resolution of the beam, we obtained information on how many secondary electrons we received from the top of the nanowires, and how many from the valleys between them. For each measurement, two points on the sample were selected, one of which corresponds to the nanowires, and the other to the sample valley between nanorods. The results of these analyses are presented in the tables below.

**Table 1:** Results obtained from thin and thick targets for MCP secondary electron detectors from tops, and between nanorods.

| **Samples** | **$R_1$** number of counts from MCP/number of pixels top of nanotubes | **$R_2$** number of counts from MCP/number of pixels between nanotubes | **$R_1/R_2$** |
|---|---|---|---|
| **Thin targets** | | | |
| ZnO/GaN (Korea) | 14.2 ± 2.8 | 4.7 ± 0.9 | 3.0 ± 0.6 |
| ZnO (Korea) | 8.4 ± 1.7 | 5.6 ± 1.1 | 1.5 ± 0.3 |
| Average | | | 2.3 ± 0.5 |
| **Thick targets** | | | |
| InP (Sweden) | 17.1 ± 3.4 | 4.1 ± 0.8 | 4.2 ± 0.8 |
| GaN/AlN (Poland) | 17.8 ± 3.6 | 1.5 ± 0.3 | 11.9 ± 2.4 |
| GaN(France) | 23.1 ± 4.6 | 10.9 ± 2.2 | 2,1 ± 0.4 |
| Average | | | 6.1 ± 1.2 |

**Thin Samples**

Table 1 shows results from experiments on thin targets prepared by the group in the Republic of Korea. In this case, two different samples were used: (a) ZnO nanorods with GaN coating; and (b) ZnO nanorods without coating. Experiments were repeated several times at different locations on the same sample. The scan area was 11.0 x 11.0 $\mu m^2$. The ratio of $R_1/R_2$ counts from MCP detectors between the top of nanotubes to counts from MCP detectors between the nanotubes was: (a) 3.0 ± 0.6 for ZnO/GaN; and (b) 1.5 ± 0.3 for ZnO. The ZnO/GaN sample shows higher SEE properties between the two thin samples. Large differences in the value of calculated SEE counts from the top and between the nanotubes indicates a not particularly uniform surface. All calculations for thin targets were performed for 40 selected top of nanotubes and between nanorods were comprising 100 pixels (10 x 10 pixel areas) each. Data were calculated from 4 different areas of the 512 x 512 pixels scan to monitor changes in the count rate during a single scan of the same sample. An error margin of 20% was estimated for all values from Gaussian distribution for all counts from MCP detectors from nanorods and valleys.

**Thick Samples**

Table 1 shows data obtained for thick samples developed at different laboratories. Unfortunately, due to the thickness of the samples ions were not detected by the PIN detector, and only counts from the MCP detector were monitored. In this case, it was assumed that the beam current during the experiment was constant - this is most likely associated with a large error. However, indicatively conclusions can be drawn about SEE properties from these samples. And, as shown in Table 1, the sample from Poland of GaN/AlN grown on thick Si (111) substrate shows a much higher reading of $R_1/R_2$ = 11.9 ± 2.4 than other samples. All calculations for thick targets were performed for 40 selected top nanorods and between nanorods comprising of 100 pixels (10 x 10 pixel areas) each. Data were calculated from 4 different areas of the 512 x 512 pixel scan to monitor changes in the count rate during a single scan of the sample. Samples of the InP and GaN shows $R_1/R_2$ = 4.1 ± 0.8 and $R_1/R_2$ = 2,1 ± 0.4, respectively. Again, the error of 20% was estimated for all values.

**Table 2:** Comparison of secondary electron emission (SEE) between different materials

| Sample | Total time [s] | Pixel dwell time [µs] | Counts from MCP detector from 4000 pixels [counts] | Number of normalized counts from MCP detector [count/pixels•µs] x$10^{-6}$ |
|---|---|---|---|---|
| ***Thin samples*** | | | | |
| Au[21:51:13] | 184.78 | 1000 | 4,547 | 4.5 ± 0.9 |
| ZnO [21-06-28] Korea | 315.19 | 1000 | 12,203 | 12.2 ± 2.4 |
| ZnO [21-15-57] Korea | 96,45 | 50 | 1,985 | 39.7 ± 7.9 |
| ZnO [21-19-26] Korea | 294,91 | 1000 | 10,911 | 10.9 ± 2.2 |
| | | | | 20.9 ± 4.2 |
| ZnO/GaN [19-23-09] Korea | 34,83 | 500 | 2,178 | 4.4 ± 0.9 |
| ZnO/GaN [19-31-37] Korea | 34,54 | 500 | 2,267 | 4.5 ± 0.9 |
| ZnO/GaN [19-33-36] Korea | 357,38 | 500 | 25,541 | 51.1 ± 10.2 |
| ZnO/GaN [19-42-57] Korea | 357,39 | 500 | 24,167 | 48.3 ± 9.7 |
| ZnO/GaN [21-33-15] Korea | 370,36 | 1000 | 16,951 | 17.0 ± 3.4 |
| Average value for thin nanomaterials | | | | 25.1 ± 5.0 |
| ***Thick samples*** | | | | |
| InP [13:49:14] Sweden | 184,72 | 100 | 8,744 | 87.4 ± 17.5 |
| InP [13:56:33] Sweden | 302,77 | 1144 | 21,395 | 18.7 ± 3.7 |
| InP [14:06:06] Sweden | 302,77 | 1144 | 21,206 | 18.5 ± 3.7 |
| | | | | 41.5 ± 8.3 |
| GaN/AlN [14:23:08] Poland | 302,77 | 1144 | 17,786 | 15.5 ± 3.1 |
| GaN/AlN [14:31:38] Poland | 302,77 | 1144 | 17,695 | 15.5 ± 3.1 |
| | | | | 15.5 ± 3.1 |
| GaN [14:46:09] France | 396,12 | 1500 | 23,061 | 15.4 ± 3.1 |
| Mean value for all nanomaterials | | | | **23.4 ± 4.7** |

Table 2 shows results of the SEE properties between different materials, including Au. In this table, the number of counts registered by the MCP detector are shown collected from the top of nanorods. In each sample, 40 randomly allocated nanorods were selected, and a number of counts were added. Again, data were calculated from 4 different areas of the 512 x 512 pixels scan to monitor changes in the count rate during a single scan of the sample. For each nanorod we selected an area of 10 x 10 pixels. For a scan area of 11.0 x 11.0 $\mu m^2$ and an area of 512 x 512 pixels, each pixel has dimensions of 21.5 x 21.5 $nm^2$. In order to prepare this table, we assumed that the beam current was stable during the experiment. This assumption is likely the largest source of error. However, Table 2 indicates that all nanomaterials show an average (23.4 ± 4.7) x $10^{-6}$ [count/pixels•μs] versus (4.5 ± 0.9) x $10^{-6}$ [count/pixels•μs] for Au; a factor of 5.2 higher in average for nanomaterials. This value alters for different samples, and even for different scans of the same sample, as indicated in Table 2. The estimated error was 20% for all presented values.

**Conclusions and Prospects**

There are several conclusions from the analysis of the results obtained: (a) the material with the highest SEE performance is a GaN/AlN thick sample, as shown in Table 1. The GaN from France and InP from Sweden indicated in Table 1 shows lower results. Most of the secondary electrons originate from the top of nanotubes in each sample, not from the valley between nanotubes.

By increasing the area of nanotubes with a higher density, it will be possible to modify SEE properties. Furthermore, it will be possible to obtain materials with higher SEE properties when compared with traditionally used Au or CsI.

There are still many parameters of 1D and other nanomaterials that should be studied in detail for SEE properties, including (a) manufacturing processes, and (b) geometry (e.g., density, length and orientation) of nanotubes.

All experimental techniques used in the works[9,10] are different to avoid possible systematic errors associated with a single technique.

In our works we used large beams with a current below 10 fA. Such current and beam density is too low to cause any damage to the sample. We have observed this fact by using the same sample over a long period of time, for more than 10 years, in different experiments at various facilities. Experiments with larger currents in the order of pA or nA will be able to resolve the question/problem about sample stability and resistance to radiation damage.

As stated in the Introduction, minimal research has been performed on the SEE properties of novel nanomaterials. Hence, we are careful not to draw detailed conclusions from our observation with the high resolution proton microprobe research at CIBA in Singapore. In our recent work[33] we developed a simple picture about the behavior of secondary electrons generated by heavy ions.

It is obvious that theoretical simulations will help in understanding the behavior of SEE properties of different nanomaterials, and be a guide for upcoming experiments. Therefore, we have already started on work to develop such a model in the near future.

**References**


[1]Ghosh S., Karmakar P. "In-situ analysis of ion-induced physicochemical change of Si surface by secondary electron yield detection", *Nuclear Inst. and Methods in Physics Research. B* 441, 56–62 (2019), https://doi.org/10.1016/j.nimb.2018.12.055.

[2]Hewei Zhao, Xiangjun Chen, Guangzhen Wang, Yongfu Qiu and Lin Guo, Two-dimensional amorphous nanomaterials: synthesis and applications, *2D Materials*, Vol. 6, No 3 032002 (2019), https://doi.org/10.1088/2053-1583/ab1169.

[3]Yongping Fu, Haiming Zhu, Jie Chen, Matthew P. Hautzinger, X.-Y. Zhu and Song Jin, Metal halide perovskite nanostructures for optoelectronic applications and the study of physical properties, *Nature Reviews Materials*, Vol. 4,169–188 (2019), https://doi.org/10.1038/s41578-019-0080-9.

[4]Y.B. Li, Y. Bando, D. Golberg, "ZnO nanoneedles with tip surface perturbations: Excellent field emitters", Appl. Phys. Lett., Vol. 84, No. 18 (2004) 3603-3605, https://doi.org/ 10.1063/1.1738174.

[5]T. Kamiya, M. Cholewa, A. Saint, S. Prawer, G.J.F. Legge, J.E. Butler, D.J. Vestyck, „Secondary Electron from B Doped Diamond under Ion Impact: Applications in Single Ion Detection", *Appl. Phys. Lett. Vol.* 71 (13) (1997) 1875-1877, https://doi.org/10.1063/1.120190.

[6]M. Cholewa, E. Koshchiy, Thin diamond film as highly efficient detector for charged particles. GSI Scientific Report 2003 (www.gsi.de) (2004) 156.

[7]M. Cholewa, B. Fischer, International Patent: PCT/EP 03/02323; P179 (GSI 12283) 2003. "Device for charged particle and photon detection" – DE 202 03 702.9.

[8]M. Cholewa, H. O. Moser, L. Huang, Shu Ping Lau, Jinkyoung Yoo, Sung Jin An, Gyu-Chul Yi, Gao Xingyu, A.T.S. Wee , A. Bettiol, F. Watt, B. Fischer, "Secondary Electron Emission Properties of III-nitride/ZnO coaxial heterostructures under ion and X-ray bombardement", Nucl. Instrum. & Meth. B Vol. 254 (2007) 55-58, https://doi.org/10.1016/j.nimb.2006.09.014.

[9]Marian Cholewa, Shu Ping Lau, Gyu-Chul Yi ,Yoo Jin Kyoung, Adrian P. Burden, Lei Huang, Gao Xingyu, Andrew T.S. Wee, Herbert O. Moser, "Radiation Detector Having Coated Nanostructure and Method", United States Patent No. 7,388,201 (June 17, 2008)

[10]P. Boutachkov, K. O.Voss, K. Lee, M. S. Song, C.Yi, M. Cappellazzo, W. Kondziołka, A. Liskowicz, M. Cholewa, „An investigation of secondary electron emission from ZnO based nanomaterials for future applications in radiation detectors", Scientific Reports, 11:737 (2021), https://doi.org/10.1038/s41598-020-80788-y

[11]R.Valizadeh, O. B. Malyshev, S.Wang, S. A. Zolotovskaya, W. A. Gillespie, and A. Abdolvand, „Low secondary electron yield engineered surface for electron cloud mitigation", Appl. Phys. Lett. 105, 231605 (2014).

[12]R. Valizadeh, O. Malyshev, S. Wang, T. Sian, M. D. Cropper, and N. Sykes, „Reduction of secondary electron yield for E-cloud mitigation by laser ablation surface engineering", Appl. Surf. Sci. 404, 370 (2017).

[13]A. Krasnov, Molecular pumping properties of the LHC arc beam pipe and effective secondary electron emission from Cu surface with artificial roughness, Vacuum 73, 195 (2004).

[14]V. Nistor, L. A. González, L. Aguilera, I. Montero, L. Galán, U. Wochner, and D. Raboso, „Multipactor suppression by micro-structured gold/silver coatings for space applications", Appl. Surf. Sci. 315, 445 (2014).

[15]C. Swanson and I. D. Kaganovich, „Modeling of reduced effective secondary electron emission yield from a velvet Surface", J. Appl. Phys. 120, 213302 (2016).

[16]M. Ye, D. Wang, and Y. He, „Mechanism of total electron emission yield reduction using a micro-porous Surface", J. Appl. Phys. 121, 124901 (2017).

[17]C. Swanson and I. D. Kaganovich, "Feathered" fractal surfaces to minimize secondary electron emission for a wide range of incident angles", J. Appl. Phys. 122, 043301 (2017).

[18]Van Kan J A, Malar P, Baysic de Vera A. „The second generation Singapore high resolution proton beam writing facility", Review of scientific instruments, 83(2): 02B902 (2012), https://doi.org/10.1063/1.3662205

[19]Yao Y, Van Kan J. A. Automatic beam focusing in the 2nd generation PBW line at sub-10 nm line resolution[J]. Nuclear Instruments and Methods in Physics Research Section B: Beam Interactions with Materials and Atoms, 348: 203-208, (2015), https://doi.org/10.1016/j.nimb.2014.12.066

[20]S. Qureshi, W. Jiacheng, J.A. van Kan, Automated alignment and focusing system for nuclear microprobes, Nuclear Inst. and Methods in Physics Research B 456, 80–85 (2019), https://doi.org/10.1016/j.nimb.2019.06.040

[21]X. Xu, N. Liu, P. S. Raman, S. Qureshi, R. Pang, A. Khursheed, J. A. van Kan, Design consederations for a compact proton beam writing system aiming for fast sub-10 nm direct write lithography, Nuclear Inst. and Methods in Physics Research B (2016), https://doi.org/10.1016/j.nimb.2016.12.031

[22]J. B. Park, H. Oh, J. Park, N.-J. Kim, H. Yoon and G.-C. Yi, "Scalable ZnO nanotube arrays grown on CVD-graphene films", APL Materials 4(10), 106104 (2016), https://doi.org/10.1063/1.4964490

[23]Young Joon Hong, Jong-Myeong Jeon, Miyoung Kim, Seong-Ran Jeon, Kyung Ho Park and Gyu-Chul Yi, "Structural and optical characteristics of GaN/ZnO coaxial nanotube heterostructure arrays for light-emitting device applications", Neu Journal of Phyaics 11(12), 125021 (2009), https://doi.org/10.1088/1367-2630/11/12/125021

[24]Chul- Ho Lee, Yong- Jin Kim, Young Joon Hong, Seong- Ran Jeon, Sukang Bae, Byung Hee Hong, Gyu- Chul Yi, "Flexible Inorganic Nanostructure Light- Emitting Diodes Fabricated on Graphene Films" Advanced Materials 23(40), 4614 (2011), https://doi.org/10.1002/adma.201102407

[25]Sake Wang, Hongyu Tian, Chongdan Ren, Jin Yu and Minglei Sun, Electronic and optical properties of heterostructures based on transition metal dichalcogenides and graphene-like zinc oxide, Scientific Reports, Vol. 8, 12009 (2018), https://doi.org/10.1038/s41598-018-30614-3

[26]G. Otnes, M. Heurlin, M. Graczyk, J. Wallentin, D. Jacobsson, A. Berg, I. Maximov, M. T. Borgström,"Strategies to obtain pattern fidelity in nanowire growth from large-area surfaces patterned using nanoimprint lithography", Nano Research, Volume 9, Issue 10, pp 2852–2861 (2016), http://dx.doi.org/10.1007/s12274-016-1379-0

[27]M. Sobanska, V. G. Dubrovskii, G. Tchutchulashvili, K. Klosek, and Z. R. Zytkiewicz, Analysis of Incubation Times for the Self-Induced Formation of GaN Nanowires: Influence of the Substrate on the Nucleation Mechanism, Cryst. Growth Des., 16, 7205−7211 (2016), https://doi.org/10.1021/acs.cgd.6b01396

[28]K. Klosek, M. Sobanska, G. Tchutchulashvili, Z. R. Zytkiewicz, H. Teisseyre, L. Klopotowski, Optimization of nitrogen plasma source parameters by measurements of emitted light intensity for growth of GaN by molecular beam epitaxy, Thin Solid Films 534, 107–110 (2013), https://doi.org/10.1016/j.tsf.2013.02.013

[29]A. Reszka, A. Wierzbicka, K. Sobczak, U. Jahn, U. Zeimer, A. V. Kuchuk, A. Pieniążek, M. Sobanska, K. Klosek, Z. R. Zytkiewicz and B. J. Kowalski, Influence of the local strain on cathodoluminescence of GaN/AlxGa1-xN nanowire structures, J. Appl. Phys 120, 194304 (2016), https://doi.org/10.1063/1.4968004

[30]M. Sobanska, N. Garro, K. Klosek, A. Cros and Z. R. Zytkiewicz, Influence of Si substrate preparation procedure on polarity of self-assembled GaN nanowires on Si(111): Kelvin Probe Force Microscopy studies, Electronics 9, 1904 (2020), https://doi.org/10.3390/electronics9111904

[31]A. Wierzbicka, Z. R. Zytkiewicz, S. Kret, J. Borysiuk, P. Dluzewski, M. Sobanska, K. Klosek, A. Reszka, G. Tchutchulashvili, A. Cabaj, and E. Lusakowska, Influence of substrate nitridation temperature on epitaxial alignment of GaN nanowires to Si(111) substrate, Nanotechnology 24, 035703 (2013), https://doi.org/10.1088/0957-4484/24/3/035703

[32]M. Morassi, N. Guan, V. G. Dubrovskii, Y. Berdnikov, C. Barbier, L. Mancini, L. Largeau, A. V. Babichev, V. Kumaresan, F. H. Julien, L. Travers, N. Cogneau, J. C. Harmand, M. Tchernycheva, Selective area growth of GaN nanowires on graphene nanodots, Cryst. Growth Des., 20, 2, 552-559 (2020), https://doi.org/10.1021/acs.cgd.9b00556

[33]Marian Cholewa, Mario Cappellazzo, Mario Ley, Dennis Bittner, Jan Jolie, Keundong Lee, Minho Song, Gyu-Chul Yi, Plamen Boutachkov, "In Search of Nano-materials with Enhanced Secondary Electron Emission for Radiation Detectors", Scientific Reports 11:10517 (2021), https://doi.org/10.1038/s41598-021-89990-y

## Acknowledgements

This work was supported by ENSAR2-PASPAG within the European Union's Horizon 2020 research and innovation program H2020-INFRAIA-2014–2015 Grant Agreement 654002 –

ENSAR2-PASPAG. We would like to thank BMBF for financial support. MS and ZRZ are grateful for support from the Polish National Science Centre grant 2016/23/B/ST7/03745.

The authors acknowledge M. Borgström, Lund University, Sweden, for supplying the InP nanowire samples. I. M. acknowledges support from NanoLund at Lund University and MyFab. And we acknowledge W. Kondziołka from the University of Rzeszów and M. Zhaohong from National University of Singapore for their help with the experiment.

## Author Information

M. Ch., A. L., A. P., T. O., J. A. v. K, Y. X. D, P. Y. Y. A. A. B. and P. B. designed the experimental strategy, performed all experiments, analyzed data and prepared the manuscript. I. M., M. S., Z. R. Z., N. G., M. T., K. L., M. S. S. and G.-C. Y. prepared samples. P. B. and M. Ch. designed experiments and organized financial support. All authors commented on the manuscript.